

# Test results and operating configuration of the Calibration unit for the near-infrared spectropolarimeter SPIRou

S. Perruchot<sup>a</sup>, M. Hobson<sup>b</sup>, F. Bouchy<sup>c</sup>, F. Dolon<sup>a</sup>, I. Boisse<sup>b</sup>, F. Moreau<sup>a</sup>, R. Sottile<sup>a</sup>, F. Wildi<sup>c</sup> and the SPIRou team<sup>1</sup>

<sup>a</sup>Aix-Marseille Université, CNRS, Institut Pytheas-Observatoire de Haute Provence, 04870 St-Michel-l'Observatoire, France;

<sup>b</sup>Aix-Marseille Université, CNRS, LAM, 13388 Marseille, France;

<sup>c</sup>Observatoire de Genève, Université de Genève, 51 Chemin des Maillettes, 1290 Sauverny, Switzerland

## ABSTRACT

SPIRou is a new near-infrared echelle spectropolarimeter and high precision radial velocity instrument, implemented at the 3.6m Canada-France Hawaii Telescope (CFHT – Mauna Kea) in early 2018. It aims at detecting and characterizing Earth-like planets around M dwarfs and studying stellar and planetary formation in the presence of stellar magnetic field. The calibration unit, with its radial-velocity reference module, is essential to the short- and long-term precision at the level of 1 m/s.

We describe the final calibration unit that has been installed. We give technical results such as thermal background level, lamps flux level, lamps stability, and report some technical issues with their solution.

**Keywords:** calibration unit, near infrared, spectrograph, radial velocity, Fabry-Perot, spectropolarimeter

## 1. INTRODUCTION

The SPIRou spectropolarimeter [1] is on the sky since April 2018 and aims to become a leading instrument on three forefront science topics, (i) the quest for habitable Earth-like planets around very-low-mass stars, (ii) the study of the impact of magnetic fields on low-mass star and planet formation, and iii) the mass determination of transiting planets orbiting low-mass stars. Since M dwarfs are faint in the visible, SPIRou works in near-infrared wavelengths (nIR). It is optimized for accurate radial-velocity (RV) measurements on M dwarfs. The polarimetric capability is needed to measure and characterize the structure of magnetic field. Detailed discussions of the science cases are given in [2] and [3]. [4] presents the SPIRou legacy survey that is planned to begin this year.

SPIRou is designed to reach a maximum efficiency and optimum precision, by taking advantage of the heritage derived from HARPS and SOPHIE spectrographs and the Espadons/Narval spectropolarimeters. It covers a very wide single-shot nIR spectral domain (0.98-2.35  $\mu\text{m}$ ) at a resolving power of 70,000. An overview of the key aspects of SPIRou's optical and mechanical design is given in [5]. The results from the instrumental tests done during integration at IRAP, Toulouse and mounting at CFHT are detailed in [6].

Essential to the RV accuracy is the calibration unit and radial-velocity reference module, located in the Coudé room and fiber linked to the spectrograph; this calibration module was assembled between Geneva and Observatoire de Haute Provence. None of the other nIR instruments includes the spectropolarimetric capability (required for magnetic field measurements) nor the essential K band (with a large RV content for low mass stars and a large flux for embedded sources). These constraints drove a specific calibration unit for SPIRou [7].

---

<sup>1</sup>SPIRou is an international project led by France and involving the CHFT, Canada, Switzerland, Brazil, Taiwan and Portugal. The SPIRou science consortium gathers over 100 scientists from more than 30 research institutes in 11 different countries.

In this article, we describe the final calibration unit that has been tested in Toulouse. The tests in Hawaii are currently ongoing and only some preliminary results are described here. After a brief description of the calibration unit in section 2, we detail the tests done in section 3. Section 4 describes some results of particular interest such as the cold channel validation, the lamps spectra and a (minor) issue with the variable density system.

## **2. SPIROU CALIBRATION UNIT BRIEF DESCRIPTION**

The SPIROU calibration unit has been fully described in [1] in its requirements, architecture and modules. We recall here the main points.

The calibration unit has to provide calibration sources in order to perform the following calibrations: location and geometry of spectral orders, the blaze profile and spectral flat-field response (pixels response), the slit geometry, the wavelength calibration, and the simultaneous drift.

In order to correct from instrumental noise, the calibration light should follow the same path as the stellar light. In practice, it means that the calibration light passes through the Cassegrain Unit of the telescope, where the polarimeter and two fibers for the two polarizations of the light are already located. It was then decided to add a specific channel that goes directly to the spectrograph. The calibration system therefore has two outputs to feed the spectrograph through two channels (see Figure 1):

- The Cassegrain link which uses the same optical path as the target through the Cassegrain Unit,
- The Reference link which is used essentially for simultaneous drift measurement, going directly to the spectrograph slicer entrance.

The calibration unit architecture, presented in Figure 2, provides all required functionalities: independent selection of any kind of needed light source for each calibration channel (through Cassegrain unit and science fiber or directly through the spectrograph entrance) by the use of trolleys in front of lamp slots; flux adaptation for simultaneous calibration by circular variable density system on Reference channel; and thermal background limitation on Reference channel for long exposures without simultaneous calibration with the help of a cold source module.

See also the pictures of the Calibration Unit Figure 3, Figure 4 and Figure 5.

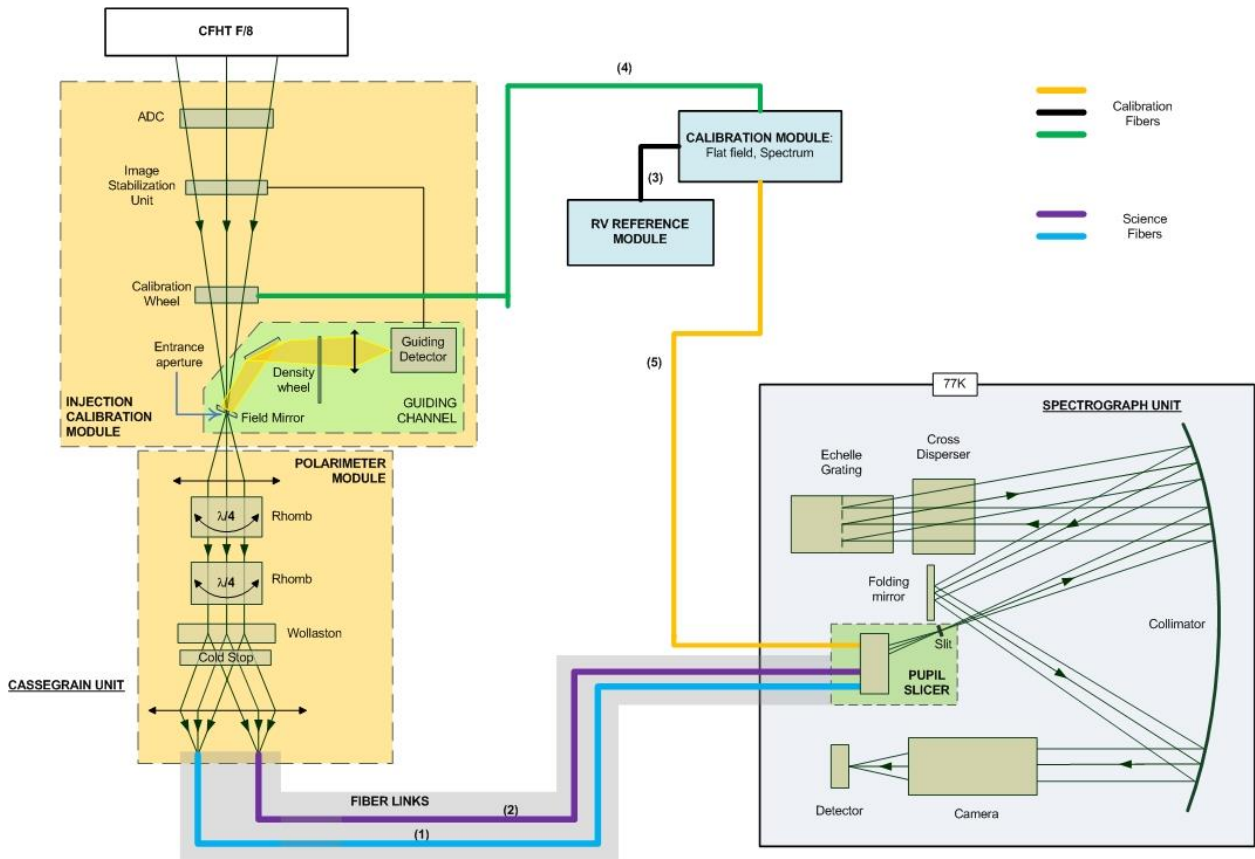


Figure 1. Architecture of the Calibration module of the SPIRou instrument. The Reference channel is a direct link from Calibration Unit to spectrograph (through the fiber slicer module), and the calibration Cassegrain channel feeds the science fibers through the Cassegrain unit. Both channels can be fed by the same or different light sources.

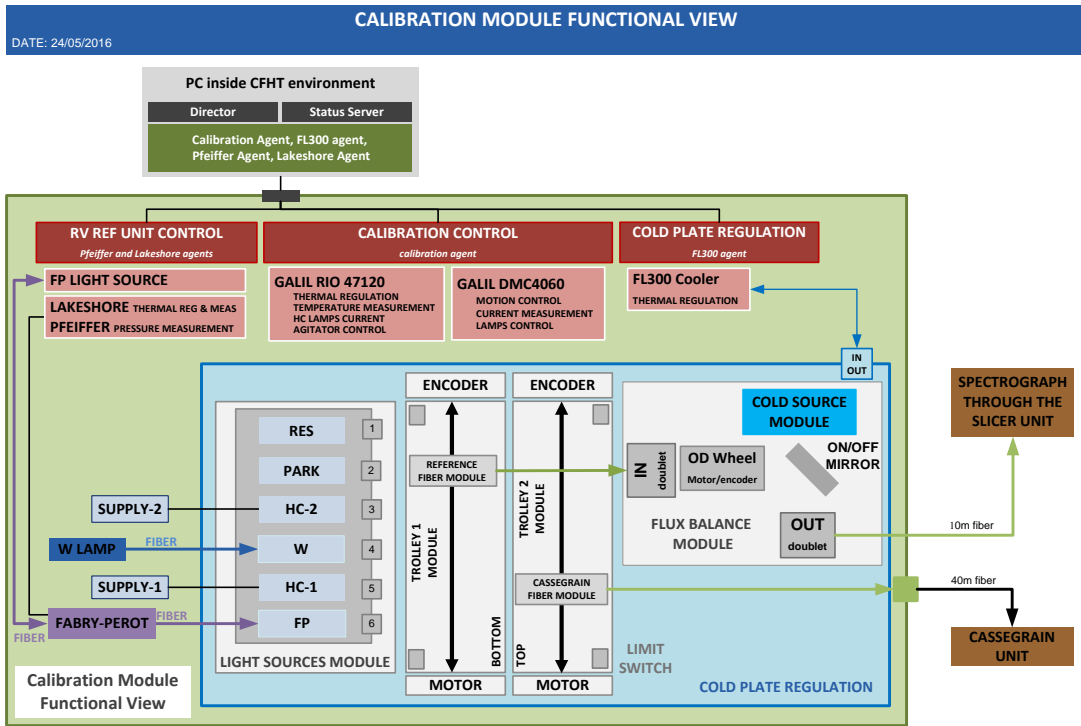


Figure 2. Calibration Unit Functional View.

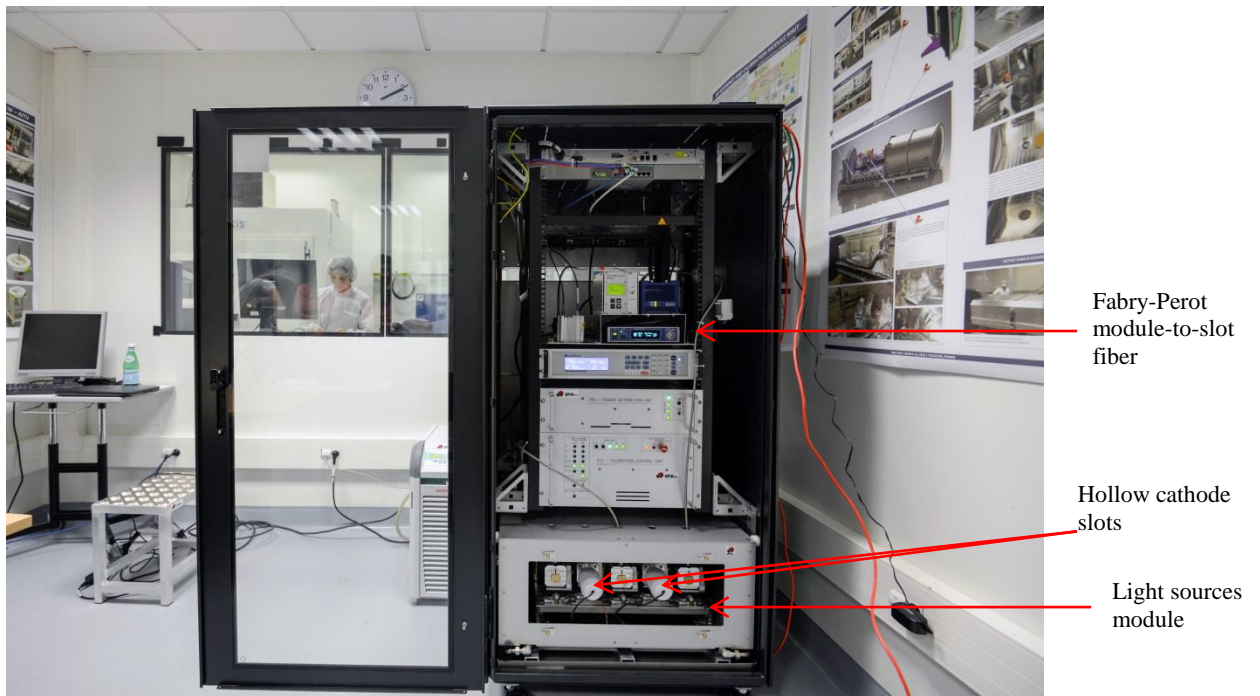


Figure 3. Calibration Unit (height 1.7m x width 0.8m x depth 1.2m) in the IRAP facility. The Fabry-Perot module is located in a more finely temperature controlled room, beside the spectrograph.



Figure 4. Electronic stages of the Calibration Unit.

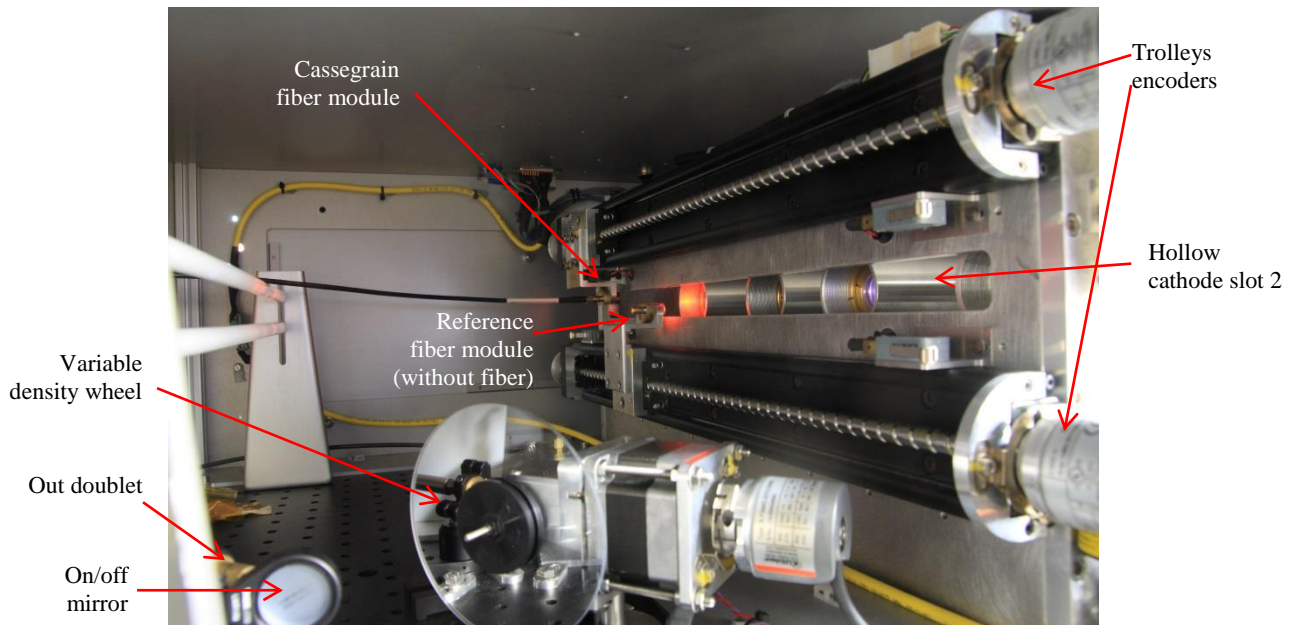


Figure 5. Picture taken during integration phase inside the Light source Module.

### 3. CALIBRATION UNIT TESTS WITH THE SPECTROGRAPH

The verification of the Calibration Unit is done following several steps. First, the Calibration Unit is tested alone, mainly functionally, but also for instance for positioning reproducibility. The two next phases requires the spectrograph, since the optical and calibration performance can only be seen with it: calibration image spectral balance, flux level, stability for instance, are properties for which the spectrograph itself is a part of the result. The first phase with the spectrograph took place in Toulouse at IRAP, where all the instrument parts (except final detector, not available at that time) were gathered and tested before delivery at CFHT. The second and final phase is at CFHT, with the final detector in the operational conditions. This last phase began in 2018 and is currently ongoing.

One difficulty is that SPIrou is forefront in the exploitation of the K band and the detector H4RG will be the first of its type and its performances are not well known at this moment. The DRS pipeline is being developed by the consortium (effort led by LAM, Marseille) and is delivered to CFHT with the instrument, aiming at a complete extraction of spectra as well as RV and polarization signatures available a few minutes after the observations.

Hence, several tests have been done at IRAP and CFHT to:

- Choose the Hollow cathode types (see §4.3). The hollow cathodes lines catalog is necessary to determine the accuracy of the wavelength solution. The definition of the catalog is an iterative process, requiring some spectral images with the definitive spectrograph system.
- Select the warming time for the HC lamps to reach the highest spectral stability.
- Select the Hollow cathode lamps supply current optimization, depending on each lamp, regarding metallic/gas flux ratio and flux stability (see [8]).
- Select the optimal exposure time for all the sources. The exposure time for the calibration should be negligible with respect to the instrumental drift time-scale (few hours) but not too short with respect to possible high frequency vibrations (few Hz). Therefore, calibration exposure time should be in between 5 and 100 s nominally and in any case shorter than 1800 s.
- Check diffused light or ghost on the spectrograph due to strong emission lines in and out of the spectral range.
- Check the thermal background on the spectrograph detector with maximal exposure time with HC source (no saturation in red orders for simultaneous reference)
- Select the white lamp for the RV reference module.
- Track any other technical issue.

When the instrument will be on the sky:

- The DRS will monitor the flux of the HC lamps that have a lifetime of around 10,000 hours. The flux increase with the ageing of the lamp. This increase could be reduced thanks to a lower supply current, but this will modify the flux ratio between the gas and the metallic lines.
- The calibrations for the determination of the location and geometry of the spectral orders, the slit geometry, the blaze profile, the spectral flat-field response and the wavelength calibration should be performed during the day to meet the requirement of time availability for observation during the night. This is possible with the assumption of an instrument drift smaller than 1 m/s during a whole night. The daily calibrations should take less than 2 hours and should be completed at least 2 hours before the start of the night. This is to prevent any permanence effects on the detector (particular sensitivity due to the CMOS detector). This is another reason to prefer the Fabry-Perot etalon to HC lamps for simultaneous calibration during the night. Emission lines of HC have important dynamics with strong gas line and we anticipate that some of them will saturate the detector.
- The complete calibration sequence will also be done at the end of the night.

At IRAP (Toulouse, France), SPIRou spectrograph was equipped with a H2RG test detector. It was smaller than the nominal one: 2048x2048 pixels of 18 $\mu$ m instead of a 4096x4096 pixels of 15 $\mu$ m. However, and despite a significant fraction (20%) of unusable pixels, it allowed us to conclude on a lot of questions on the spectrograph performance, and also on the Calibration Unit technical facts.

At CFHT (Hawaii), we benefit from the H4RG final detector implementation, with the whole image format.

We highlight here some technical tests performed in Toulouse (France): the cold channel validation (section 4.1), the spectra characterization (section 4.2), a partially solved issue with the density wheel system (section 4.5) and modal noise effect (section 4.6). The performance tests concerning more specifically the spectropolarimeter are described in [6].

## 4. MAIN TECHNICAL TEST RESULTS

### 4.1 Cold channel validation

The Reference channel permanently illuminates the spectrograph, even when no calibration is demanded. For long exposures on faint targets without simultaneous calibration, this channel should not introduce a thermal background level that may pollute the science spectra. Therefore the thermal flux from the reference link should be smaller than around 30 ph/s/Å at spectrograph entrance.

A dedicated channel has been designed to reach such a level, minimizing the number of contributing elements, by the use of a flip mirror flipping from calibration light sources to a Cold channel. Two concepts were possible: using the Narcissus effect with the SPIRou detector or creating a cold source. This last concept has been preferred. The cold source module is composed of a surface with a high emissivity (Black Acktar) placed in a cell at low temperature (-25°C) closed by a very transmissive especially coated window in the thermal wavelength range. The cold target is viewed by the Reference fiber and then the spectrograph through a specific CaF<sub>2</sub>/SFTM16 doublet to minimize the absorbance factor. This last element is also coated to minimize infrared losses and also the possible straylight. As it is mounted on the thermally controlled breadboard (12°C), it benefits from its low temperature to reduce its residual thermal emission. The fluoride fiber linking to the spectrograph is of high quality and designed with a reduced Numerical Aperture of 0.15 to reduce its thermal background (see [9]).

The predicted flux at 2.35 $\mu$ m is roughly calculated using the blackbody formulae and the fiber thermal emissivity model developed in [9] and the module is expected to reach the performance goal without margin in operational conditions.

At Toulouse, during the first test phase before the final focus step, we compared different instrumental configurations to validate our choice and better understand the influence of different contributors: cold part viewed by the Reference channel (the dedicated nominal Acktar Module with a high emissivity, or a brilliant similar module (Narcissus mode, but with potentially more straylight), or a park position as a slot (adding two doublets and a short fiber); different temperatures for the Cold part to directly observe its efficiency with respect to the temperature and estimate external straylight; different temperatures of the Cold breadboard giving their temperature to all optics.

A 5 minutes exposure was taken for each configuration. The analysis gives the mean value of a horizontal cut at intersection with the last and last but one orders (2.48 $\mu$ m and 2.4  $\mu$ m at order center), where there is the highest thermal signal, on 20 lines excluding dead pixels (Figure 6).

The results are shown in Figure 7. The Acktar configuration with the nominal temperature is the best one as expected, and is therefore definitively implemented. The brilliant module, much less emissive, seems to send more straylight coming from the module environment. The  $-25^{\circ}\text{C}$  Cold part temperature is efficient, but no significant improvement is expected by reducing it – it is not worthwhile to complicate the system, which is limited by the Peltier structure used (see Figure 8). We can also see the advantage of a cold breadboard cooling the optics and the environment.

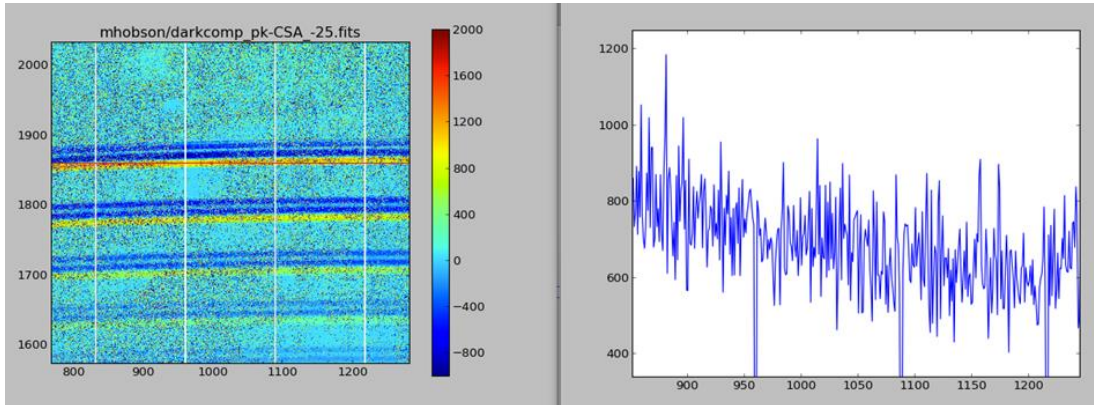


Figure 6. Thermal background image zoomed on the last orders with the test detector with a high rate of dead pixels (left). Row cut used for the analysis to estimate the level (mean value on 20 lines excluding dead pixels), same location for all configurations (right).

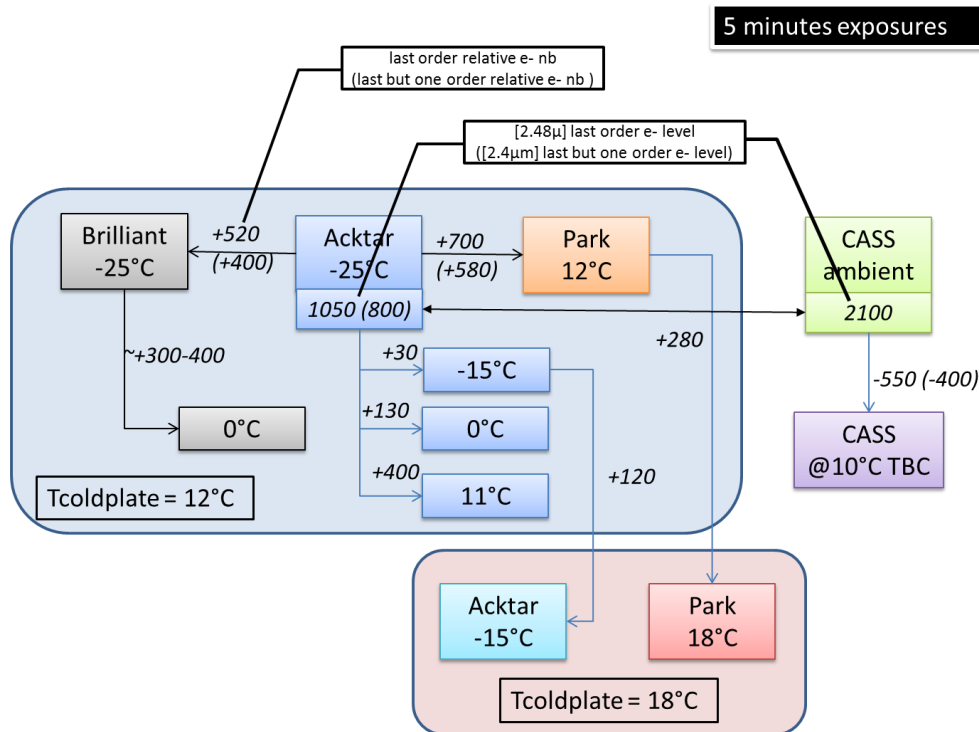


Figure 7. Cold channel configurations test summary. For each experimental configuration, estimation of the electrons level on the two last orders, relative to the nominal configuration (Black Acktar cold part at  $-25^{\circ}\text{C}$ ), are given.

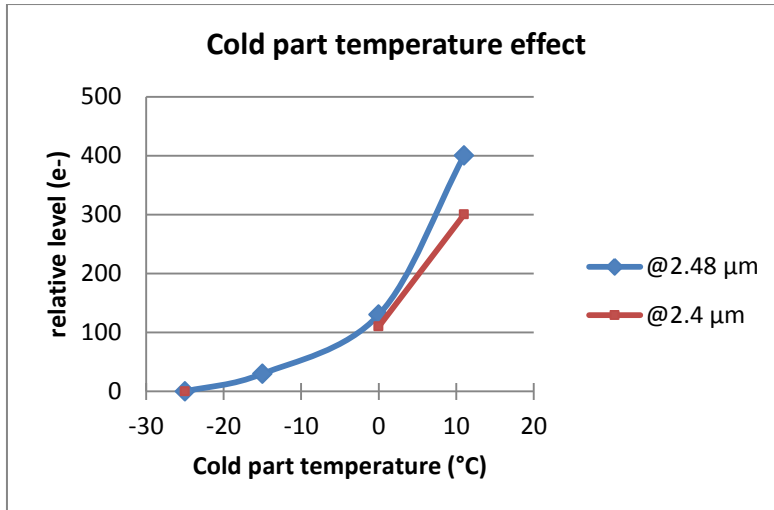


Figure 8. Cold part temperature dependence test with Acktar black module. Relative e- level in one pixel compared to the nominal -25°C configuration function of cold part temperature for the two last orders. 5 minutes exposure, Cold plate temperature 12°C.

The predicted level with the experiment conditions was  $45.5 \text{ ph/s/}\text{\AA}$  @2.35 $\mu\text{m}$ . The measured level is estimated with some hypothesis (detector QE) and high uncertainty to  $\sim 80 \text{ ph/s/}\text{\AA}$ . This is not too far from the prediction, less than a factor 2. Furthermore, we identified at least the spectrograph entrance structure as a thermal contributor (with images with no fibers connected), which was not included in the predicted flux.

The Cold channel flux level will then be measured with the final detector in Hawaii in the nominal operation conditions for final validation.

#### 4.2 Spectra location and blaze profile: continuum spectra

The continuum spectra (Figure 9), generated with a tungsten lamp, are used to locate the spectra and extract the blaze profile (Figure 10). Exposures of a few seconds are sufficient to obtain a high SNR on the useful wavelength domain (Figure 11) with a dynamic range of about 8 between the blue and the red part.

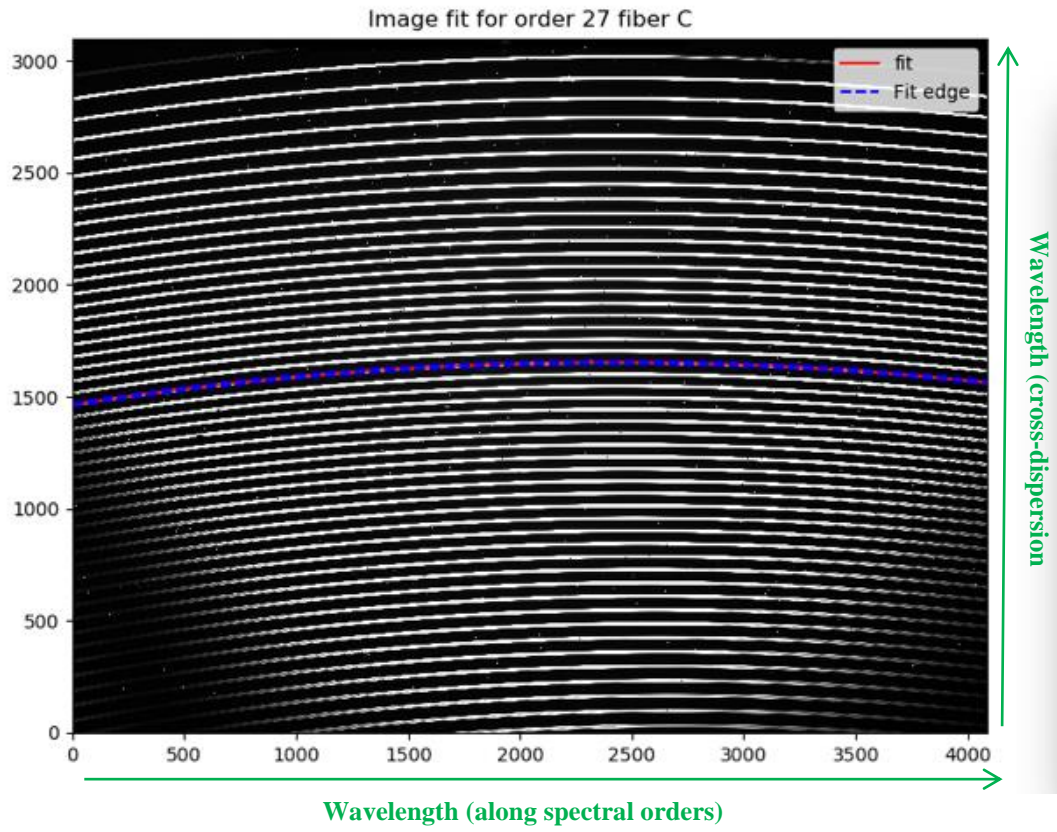


Figure 9. Tungsten lamp image providing the 49 spectral orders location.

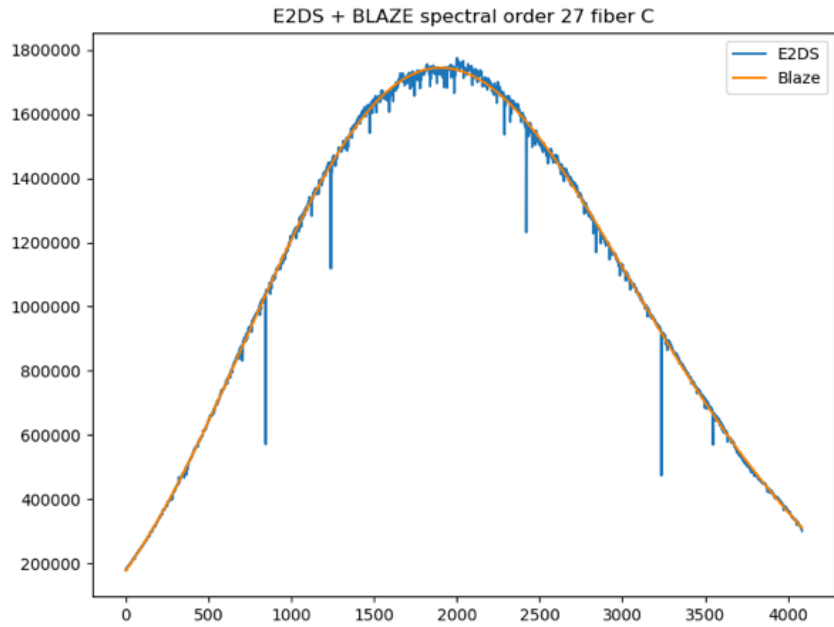


Figure 10.Extraction of a white spectrum order (#27) to determine the blaze function.

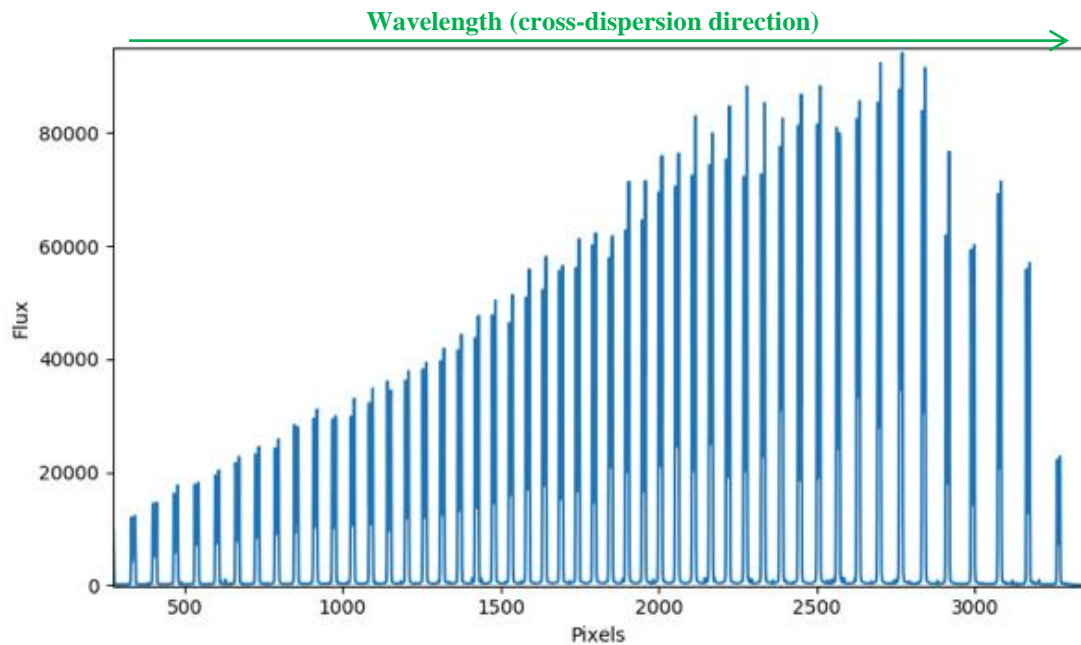


Figure 11.Cut across the orders at blaze center for a 33seconds Tungsten lamp exposure on Reference channel. Flux ratio ~8 between the shortest and the longest wavelengths.

### 4.3 Wavelength calibration: Hollow cathodes

The SPIRou calibration unit possesses three lamps for wavelength calibration: two hollow-cathode (HC) lamps, UNe and ThAr, and a Fabry-Perot etalon. The HC spectra provide lines whose absolute wavelength is known to high precision,

but which vary greatly in spacing and flux levels, while the FP provides evenly spaced lines of similar intensity but whose wavelength must be calibrated. By combining these two lamps (on average about 60 U lines and 500 Fabry-Perot lines per order), we aim to achieve a wavelength solution accurate to 0.45 m/s.

For the HC lamps, we employ the catalogs of [10] and [11]. A first limitation of these catalogs is that they do not extend across the full spectral domain of SPIRou, stopping at 2.4  $\mu\text{m}$  (UNe) and 2.34 $\mu\text{m}$  (ThAr) respectively; however, the FP can be used to bridge the final order. Spectra were obtained for both lamps at IRAP with the H2RG test detector (Figure 12). Estimated order coverage was used to manually match catalogued lines to the extracted spectra, generating a first-guess solution to which iterative algorithms could be applied. Both HC lamps spectra show numerous strong lines which are not present in the catalog (Figure 13). The UNe lamp proved to have far more identifiable lines than the ThAr, so efforts for the wavelength solution were focussed on this lamp. The catalog was filtered to remove blended lines. The drift of each line over time was also measured, and outlying lines were removed.

The level of bad pixels on the H2RG detector meant that many low-intensity lines proved hard to fit accurately, limiting the precision of the wavelength solution based on HC lamps alone. Therefore, we decided to also incorporate FP lines into the wavelength solution. The solution derived from the HC lines is used to provide an approximate solution for the FP lines, which is corrected following the procedure of [12]. The FP lines and the HC lines are then grouped together as a single input to the iterative process. With this approach, we were able to achieve a precision of 1.5 – 2 m/s, primarily limited by factors related to the H2RG detector (bad pixels, incomplete spectral domain coverage, etc). We are confident that the required precision will be achievable with the H4RG detector.

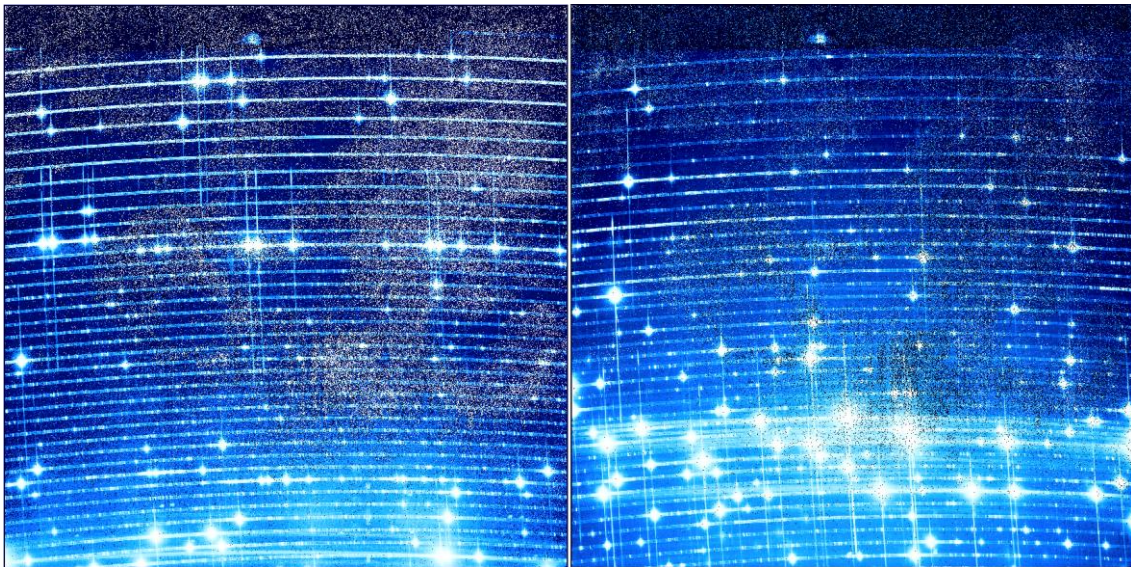


Figure 12: HC lamp spectra obtained at Toulouse with the H2RG detector (UNe on left, ThAr on right).

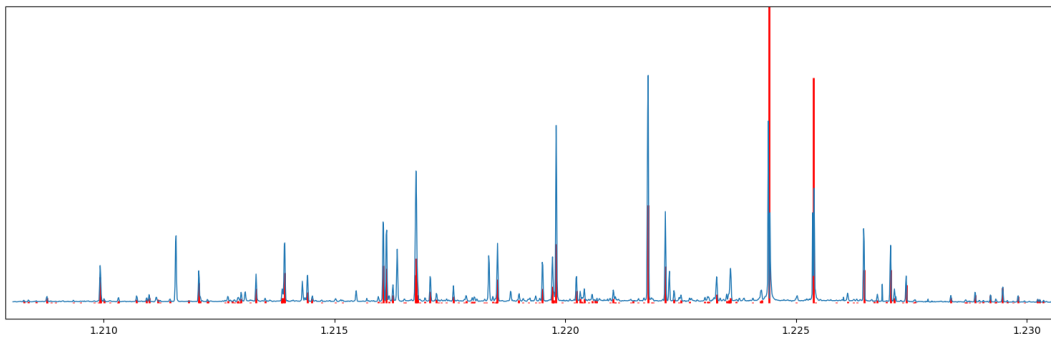


Figure 13: A wavelength-calibrated spectral order for the UNe lamp (in blue) with catalogue lines indicated (in red). Several strong lines in the spectra have no corresponding catalogue line.

#### 4.4 Drift follow-up: Fabry-Perot spectra

The Fabry-Perot etalon provides a large number of ultra-stable lines to follow the instrument drift. It is fed by an LDLS lamp or a Tungsten lamp (less brilliant). Figure 14 shows an extracted order of the Fabry-Perot spectrum, with its high line density. An example of drift follow-up sequence is presented in Figure 15: the difference in RV measurements between science channels (A and B) and the reference channel (C) is less than 30 cm/s on 42 hours, which is very encouraging.

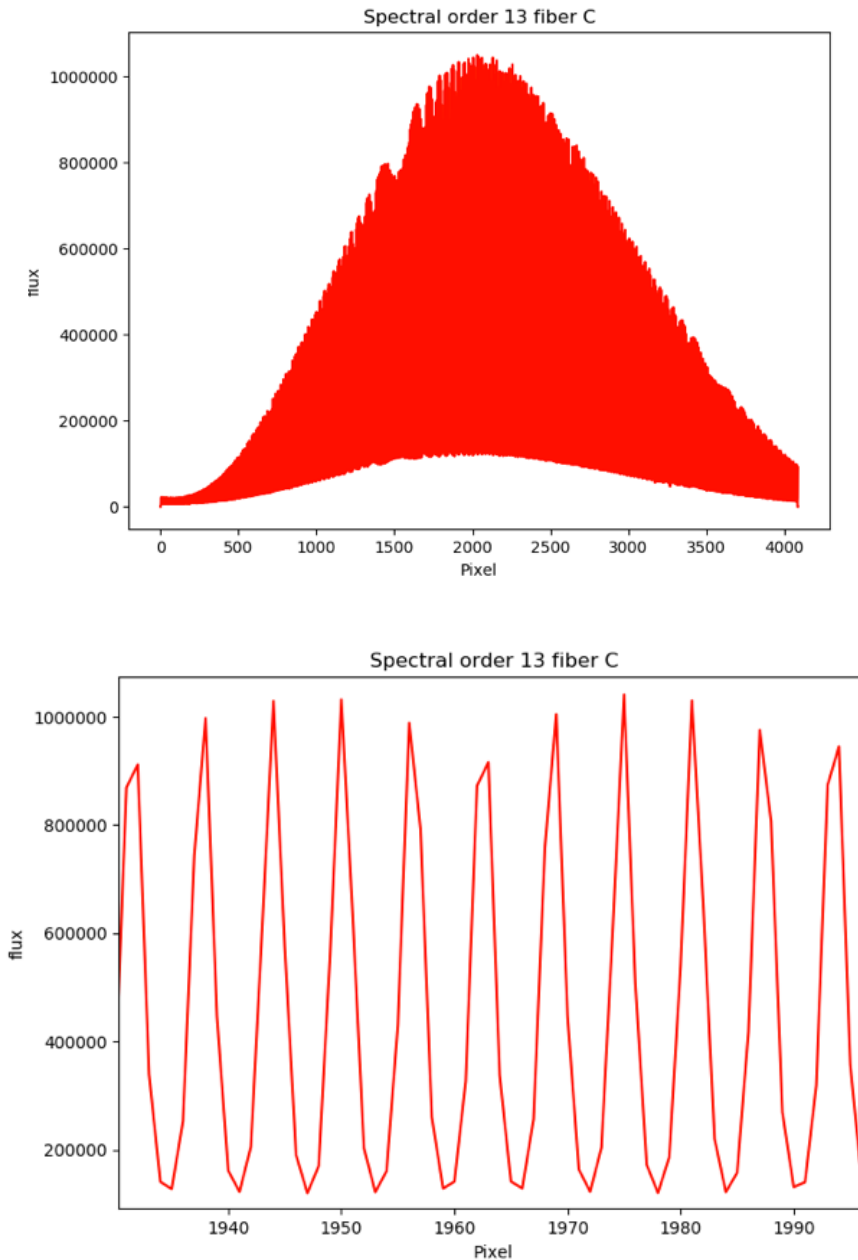


Figure 14: Top: Extraction of the 13<sup>th</sup> order Fabry-Perot spectrum, from a 600s exposure of the Fabry-perot source fed with an LDLS lamp. Bottom: Zoom showing a high flux level (saturation from 100s only on this order). Photon noise on the drift calculation is estimated to only a few cm/s.

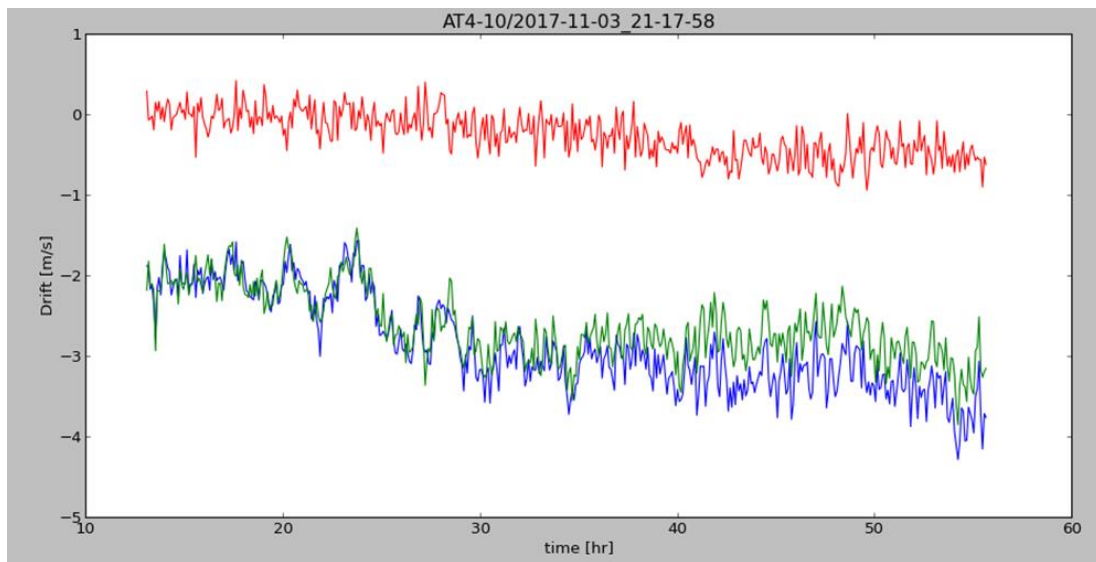


Figure 15. Drift of the spectrograph measured with a sequence of Fabry-Perot lasting 42 hours. Fibers AB (blue), C (green) and the difference AB-C (red) have RMS dispersion of 0.58 m/s, 0.43 m/s and 0.27 m/s respectively.

#### 4.5 Variable density wheel issues and solutions

In order to measure the instrumental drift, the science target should be observed simultaneously with the RV reference module which is nominally based on a Fabry-Perot etalon or in backup solution the Hollow-Cathode lamp. The intensity level of the RV reference system should be adjusted as function of the exposure time of the science target in order to keep the same level of flux independently of the exposure duration. This is done by a continuous variable density wheel placed on the path of a collimated beam generated by an optical relay, which images the fiber output from the slots onto the reference fiber linked to the spectrograph. The 1:1 relay is a symmetric system made of two specific doublets, the output one being also used for Cold Channel described in section 4.1. The whole system is mounted on the cooled breadboard preventing an excessive thermal background emission. The initial density system consisted of two identical counter-rotating continuous variable densities from Thorlabs NDC-100C-2 to keep the far-field homogeneous and reduce the spectral optical density difference at high OD - we measured the spectral density on different metallic fixed or variable densities and noted it diverges especially at high density (higher than OD2.2), with density decreasing with wavelength.

One issue emerged during the first test phase in France: troublesome Fabry-Perot-type fringes on the continuum spectra. The neutral density in front of the injection fiber at Tungsten source used to balance flux between Reference and Cassegrain channel has been taken off, thus removing the fringes on the Cassegrain spectra. But there were still fringes on the Reference channel, where the variable system is implemented, with a fringes period corresponding to the 2mm-thickness of the two variable density wheels. The fringes contrast (up to 15%) and phase depend on the density position. This affects the spectral flat-field extraction, but also the drift follow-up: a 3% variation along 15 pixels induces a fake drift of 6m/s. Nevertheless, the fringes are repeatable with position, allowing for an observing strategy that limits the drift effect. Another problem is the absorption of the commercial wheels material, UV fused silica, near 1.38 $\mu$ m and 2.2 $\mu$ m.

We modified the density wheel system in three aspects. First, we replaced the two wheels system by a single one, NDC-100C-4 (dynamic OD0-OD4): this reduces the depth of the two absorption bands, but with two draw-backs: illumination inhomogeneity in fiber far-field, and density value diverging at high density. Second, the conjugation of the 1:1 optical relay shaping the beam on the density was changed to open the angles of incidence and then reduce the fringes contrast,

by defocussing the output doublet by 1 mm in extrafocal for a focal length of 15 mm, and compensating the input doublet backfocus to keep a good conjugation. We verified that no negative effect appeared on the Cold Channel that passes through the defocussed output doublet. Finally, we decided to coat the density back-surface with a very high quality anti-reflection coating ( $R < 0.3\%$ ) to reduce more efficiently the fringes contrast (coating made by Thin Film Physics). This last step is pending waiting for its production. The expected contrast reduction factor is  $\sim 10$ .

Several tests were performed to characterize the fringes: flat exposures at different density positions, to evaluate the fringes contrast and phase repeatability as a function of density position and wavelength, Fabry-Perot exposures to follow the radial velocity as a function of the density position.

We present here some results obtained with one single wheel OD0-4 at Toulouse with test detector. The fringes' phase and contrast repeatability with density position is demonstrated Figure 17. The contrast increases with wavelength, which is not simply explained (Figure 16). At a given wavelength, the contrast stays stable with density position but not the phase. The calculated radial velocity drifts for several m/s for different density positions (Figure 18). Figure 19 shows that defocussing the beam is efficient: contrast reduction by a factor of 3 with 1 mm defocus for a 15 mm focal length. We then modified the relay on both sides to maintain also the flux level.

The final configuration (coated variable density, de-collimated relay) will be tested in Hawaii.

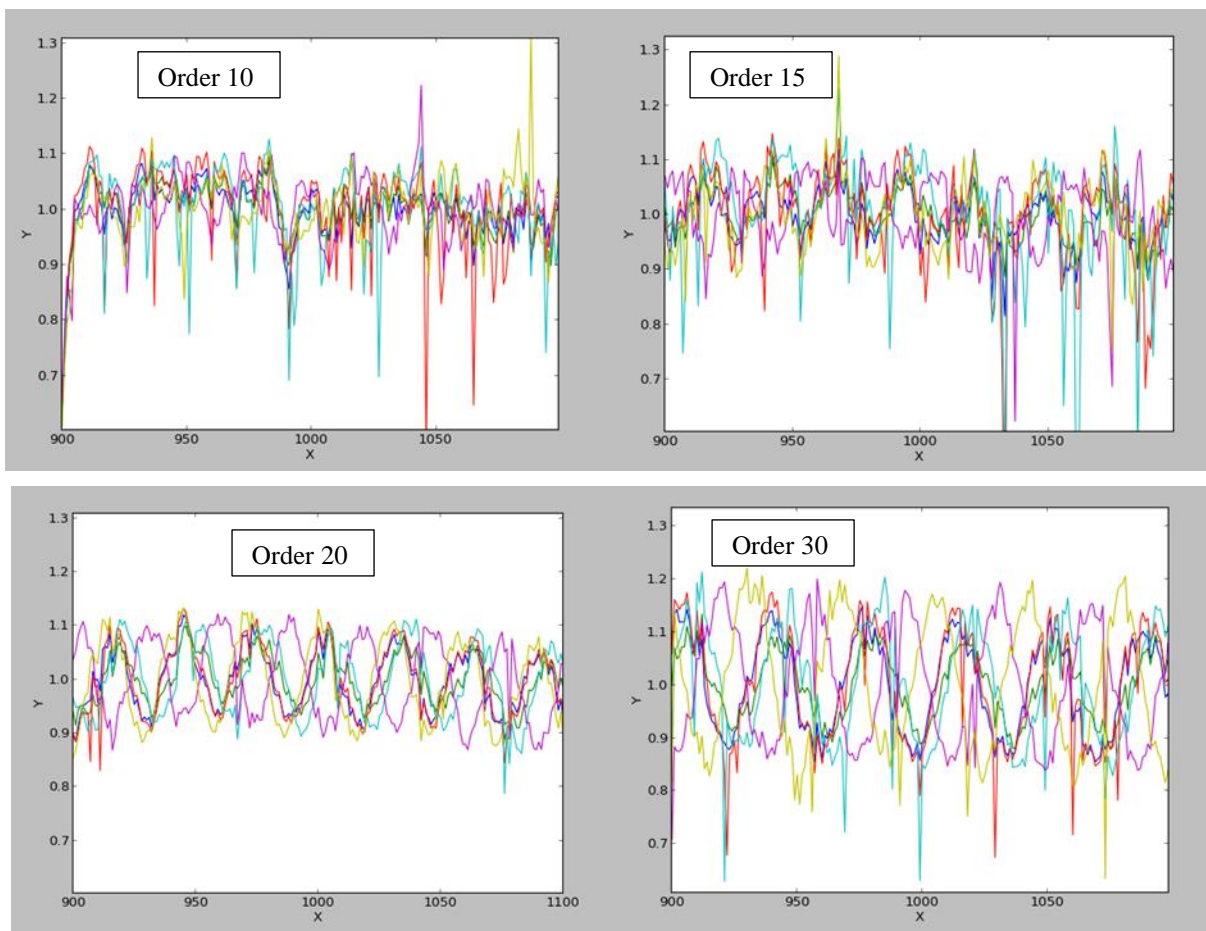


Figure 16. Fringes with flat exposures for 6 density positions near 4 orders' center. One single density wheel in collimated beam on test detector (a lot of dead pixels). Phase changes when contrast stays stable with density. The contrast increases with wavelength.

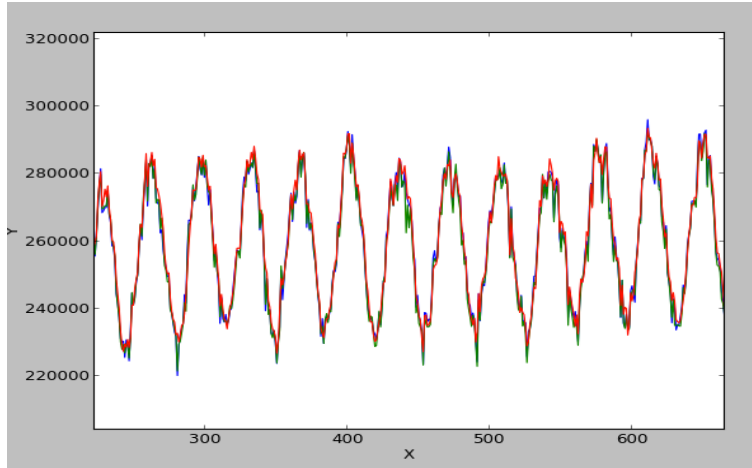


Figure 17. Very good repeatability of fringes' phase and contrast for a given density position

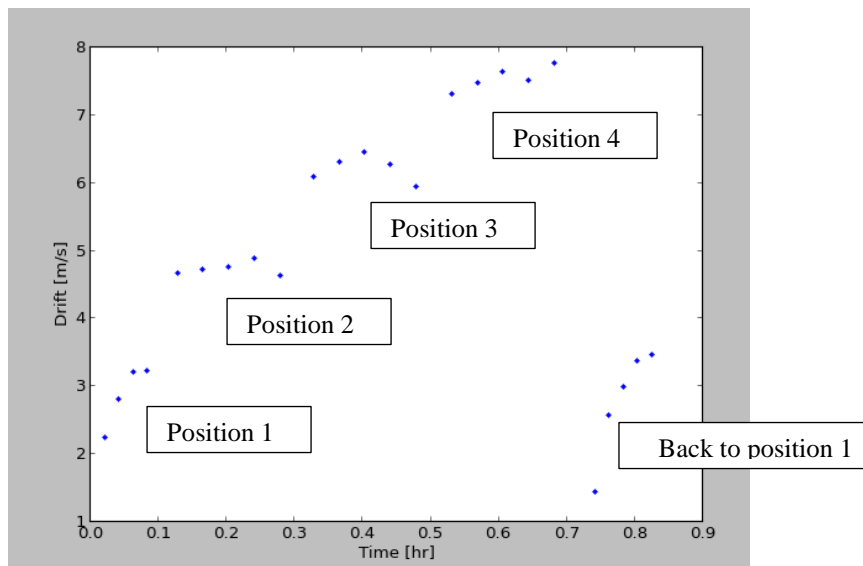


Figure 18. Radial velocity drift with density position. Fabry-Perot exposures in the configuration with one single density wheel in collimated beam on test detector.

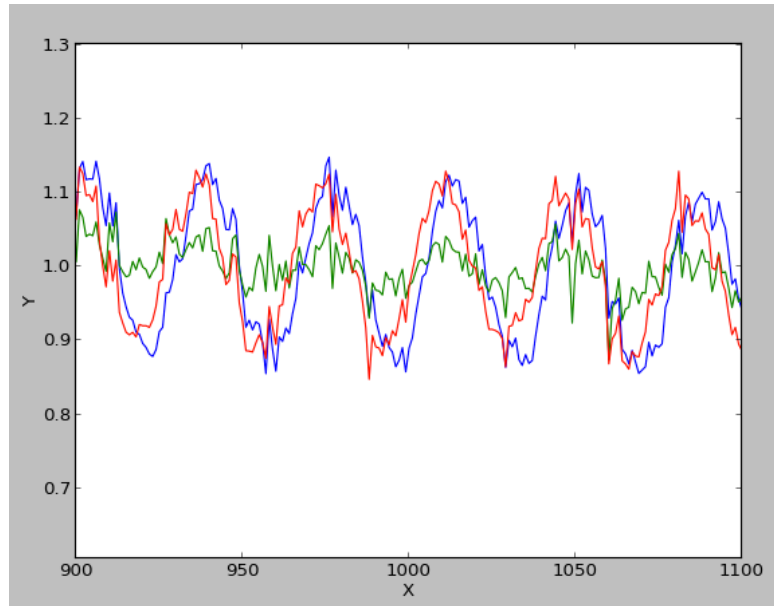


Figure 19. Contrast for three configurations on order 30: (blue) collimated beam, (red) extrafocal defocus on input doublet (green) extrafocal defocus on output doublet.

#### 4.6 Fiber modal noise

The stability of input illumination at spectrograph entrance is crucial to maintain a stable instrumental response (PSF), both in near-field (fiber output surface) and in far-field (fiber irradiance figure). Illumination changes due to instrumental instabilities induce fake drift of the signal.

Some fibers move in the SPIRou instrument (Figure 2): the two source selecting fibers in the Calibration Unit, with their injecting optics on two trolleys, and the fibers entering or exiting the Cassegrain Unit. Furthermore, some of them are in a changing thermal environment under the dome. These two factors, movement and temperature, can induce changes in light guiding in the fibers, and finally changes in the instrumental response.

During the first phase at IRAP, we took calibration images before and after calibration unit fiber movement, with or without an agitator, with continuum source or Fabry-Perot channel. It seemed that the fiber movement creates modal noise, visible on flats, and on the radial velocity drift, and that the use of a fiber agitator tends to improve signal stability. Nevertheless it was difficult to conclude with these very preliminary tests on the fiber modal noise impact. Further investigations are ongoing.

## 5. CONCLUSION AND PERSPECTIVES

Laboratory tests demonstrate that the calibration unit of SPIRou is fully compatible with the technical requirements to perform all the needed calibration of the SPIRou nIR spectropolarimeter. It also allows the derivation of radial velocity drift measurements on a short time scale below 1 m/s.

Further tests are being carried out in Hawaii to fully validate SPIRou under operating conditions. The analysis of these tests is currently ongoing, but first results are highly encouraging.

## REFERENCES

- [1] Donati, J.-F.; Kouach, D.; Lacombe, M.; Baratchart, S.; Doyon, R.; Delfosse, X.; et al., "SPIRou: A nIR Spectropolarimeter/High-precision Velocimeter for the CFHT", Handbook of Exoplanets, Edited by Hans J. Deeg and Juan Antonio Belmonte (2017). Springer Living Reference Work, ISBN: 978-3-319-30648-3, 2017, id.107 (arXiv:1803.08745)
- [2] Delfosse, X.; Donati, J.-F.; Kouach, D.; et al., "World-leading science with SPIRou - The nIR spectropolarimeter / high-precision velocimeter for CFHT", SF2A-2013: Proceedings of the Annual meeting of the French Society of Astronomy and Astrophysics (2013). Eds.: L. Cambresy, F. Martins, E. Nuss, A. Palacios, pp.497-508 (arXiv:1310.2991)
- [3] Santerne, A.; Donati, J.-F.; Doyon, R.; et al., "Characterizing small planets transiting small stars with SPIRou", SF2A-2013: Proceedings of the Annual meeting of the French Society of Astronomy and Astrophysics (2013). Eds.: L. Cambresy, F. Martins, E. Nuss, A. Palacios, pp.509-514 (arXiv:1310.0748)
- [4] Moutou, C.; Boisse, I.; Hébrard, G.; et al., "SPIRou: a spectropolarimeter for the CFHT", SF2A-2015: Proceedings of the Annual meeting of the French Society of Astronomy and Astrophysics (2015). Eds.: F. Martins, S. Boissier, V. Buat, L. Cambrésy, P. Petit, pp.205-212 (arXiv:1510.01368)
- [5] Artigau, É., Kouach, D., Donati, J.-., et al., "SPIRou: the near-infrared spectropolarimeter/high-precision velocimeter for the Canada-France-Hawaii telescope", Proc. SPIE 9147 (2014), id. 914715 (arXiv:1406.6992)
- [6] Carmona, A., et al., "SPIRou @CFHT : full in-lab and on sky performances", Proc. SPIE (2018)
- [7] Boisse, I., et al., "Calibration unit for the near-infrared spectropolarimeter SPIRou", Proc. SPIE 9908 (2016). doi: [10.1117/12.2231678](https://doi.org/10.1117/12.2231678)
- [8] Sarmiento, L. F., Reiners, A., Seemann, U et al. "Characterizing U-Ne hollow cathode lamps at near-IR wavelengths for the CARMENES survey", SPIE, 9147, 54 (2014)
- [9] Zur, A. and Katzir A., "Theory of fiber optic radiometry, emissivity of fibers and distributed thermal sensors", Appl. Opt. 30, 660-673 (1991)
- [10] Redman, S. L., Ycas, G. G., Terrien, R., et al. "A High-resolution Atlas of Uranium-Neon in the H Band", ApJS, 199, 2 (2012). doi : 10.1088/0067-0049/199/1/2
- [11] Redman, S. L., Nave, G. and Sansonetti, C. J. "The spectrum of Thorium from 250 nm to 5500 nm: Ritz wavelengths and optimized energy levels", ApJS, 211, 1 (2014)
- [12] Bauer, F. F., Zechmeister, M., Reiners, A. "Calibrating echelle spectrographs with Fabry-Perot etalons", A&A 581, A117 (2015). doi: 10.1051/0004-6361/201526462